

# Mode locking of vortex matter driven through mesoscopic channels

N. Kokubo<sup>1</sup>, R. Besseling<sup>1</sup>, V. M. Vinokur<sup>2</sup> and P. H. Kes<sup>1</sup>

<sup>1</sup>*Kamerlingh Onnes Laboratory, Leiden University, P.O.Box 9504, 2300 RA Leiden, The Netherlands.*

<sup>2</sup>*Argonne National Laboratory, Materials Science Division, 9700 South Cass Avenue, Argonne, IL 60439.*

(November 1, 2018)

We investigated the driven dynamics of vortices confined to mesoscopic flow channels by means of a dc-rf interference technique. The observed mode-locking steps in the  $IV$ -curves provide detailed information on how both the number of vortex rows and the lattice structure in each flow channel change with magnetic field. Minima in flow stress occur when an integer number of rows is moving coherently, while maxima appear when incoherent motion of mixed  $n$  and  $n \pm 1$  row configurations is predominant. Simulations show that the enhanced pinning at mismatch originates from quasi-static fault zones with misoriented edge dislocations induced by disorder in the channel edges.

74.60.Ge, 74.60.Jg, 83.50.Ha, 62.20.Fe

During the last decades, vortex matter in superconductors has been widely recognized as model system for investigating driven, periodic media in various pinning potentials. One of the intriguing phenomena it can display is a non-monotonous behavior of the depinning current density  $J_c$  with magnetic field. The best known example of such behavior is the so called peak effect occurring in weak pinning superconductors near  $H_{c2}$  [1]. Non-monotonous behavior of  $J_c$  also occurs in superconductors with (artificial) periodic pinning arrays due to the possibility of (in)commensurability between the pinning structures and the vortex arrays [2]. In both cases, the change in  $J_c$  is accompanied by pronounced structural transitions in the static as well as the driven "lattice". For periodic pinning, it was predicted theoretically [3] and confirmed by experiments [4] that defects due to incommensurability can cause a drastic reduction of  $J_c$ . For the case of the peak effect in presence of random pinning the consensus is that the opposite happens: here plastic deformations cause an *increase* in  $J_c$ . However, the role of defects in the plastic flow regime above the pinning threshold remains largely unknown.

A powerful tool to obtain time averaged, small scale information on the moving structure is to probe the dc current-voltage ( $I$ - $V$ ) characteristics in presence of superimposed rf-currents [3,5,6]. When a vortex lattice moves *coherently* at average velocity  $v$  through a pinning potential, a microscopically periodic velocity modulation [7] is induced at the washboard frequency  $f_{int} = v/a$  and, generally, at integer multiples  $qf_{int}$ . Here,  $a$  is the lattice period *in the direction of motion*. In presence of an rf-force with frequency  $f$  these modulations get mode-locked when  $f_{int}/f = p/q$  where  $p$ , like  $q$ , is an integer, giving rise to interference plateaus in the  $I$ - $V$  curves. The appearance of this phenomenon was shown to depend sensitively on the structure of the moving lattice [8].

In this Letter we report the results of mode-locking experiments on vortex matter driven through mesoscopic channels. The channel device [9] consists of an amor-

phous (a-)Nb<sub>x</sub>Ge<sub>1-x</sub> film ( $x \simeq 0.3$ ,  $T_c = 2.68$  K and thickness  $d = 550$  nm) with a NbN film ( $T_c = 12$  K,  $d = 50$  nm) on top. Straight parallel channels (width  $w = 230$  nm and length  $300 \mu\text{m}$ ) were etched in the NbN layer. Pinning in a-NbGe is very weak, while in NbN it is very strong [10], providing easy vortex flow channels with strong pinning channel edges (CE's) (see lower inset to Fig. 1). Importantly, the structure of vortex matter in the channel can be tuned on the 'atomic' scale by changing, through the applied field, the (mis)matching conditions between the lattice period and channel width.

In our system the dc-critical current at which vortices in the channel start to move is determined by the (*shear*) *interaction with pinned vortices in the CE's*. Phenomenologically,  $J_c$  follows from  $F_c = J_c B = 2Ac_{66}/w_{eff}$  [9], with  $F_c$  the critical force density,  $B$  the induction,  $c_{66}$  the vortex lattice shear modulus and  $w_{eff}$  the effective channel width. The parameter  $A$  depends crucially on the microscopic structure of the vortex arrays. In fields for which the arrays in the channel and the CE's are commensurate ( $a = a_0$  and  $w_{eff}/b_0$  integer in the inset to Fig. 1 with  $a_0 = 2b_0/\sqrt{3} = (2\Phi_0/\sqrt{3}B)^{1/2}$  the equilibrium lattice spacing), one expects a large flow stress, whereas it should be small for incommensurate fields due to the occurrence of misfit dislocations [11]. This picture seems correct, since  $J_c$  shows oscillations and is globally proportional to  $c_{66}$  [9]. However, recent studies [12] indicate that this picture is very sensitive to positional disorder of the vortex arrays in the CE's, particularly when this disorder is sufficient to cause spontaneous formation of dislocations. Recent STM experiments [13] on vortices in NbN indeed show strong deviations from the regular lattice arrangement.

This new ingredient turns out to have intriguing consequences. By means of the mode-locking technique we were for the first time able to determine unambiguously the number of moving vortex rows, the evolution of the microstructure and, from simulations, the microscopic origin of the flow-impedance oscillations in the channels.

The measurements were performed in a conventional four-probe geometry. The rf-current was applied through an rf-transformer with balanced transmission lines and a matching circuit. We used frequencies from 1 to 200 MHz and amplitudes  $I_{rf} < 5$  mA. To avoid heating, the sample was immersed in superfluid  $^4\text{He}$ . All data shown here was obtained at  $T = 1.9$  K. Since strong field-history effects exist [9], we focus for simplicity on results of field down measurements where first a field  $\sim \mu_0 H_{c2}$  of NbGe is applied after which we slowly ( $\mu_0 dH/dt \simeq -2$  mT/s) sweep to the field under consideration.

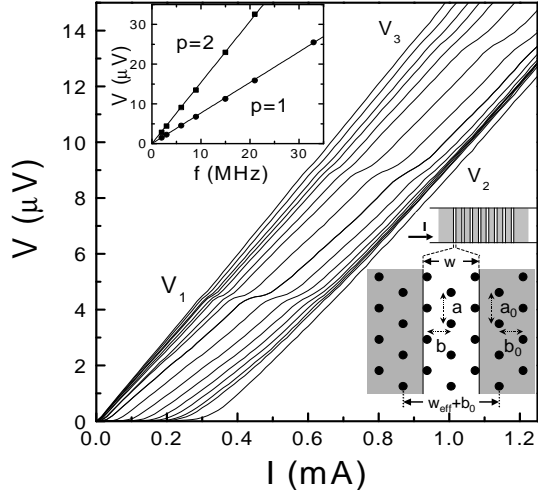


FIG. 1. Main panel: dc-IV curves at 60 mT measured with superimposed 6 MHz rf currents (amplitude 4.7, 3.8, 3.0, 2.4, 1.9, 1.5, 1.2, 0.94, 0.75, 0.59, 0.47, 0.38, 0.30, 0.24, 0.19, 0.15 and 0 mA from left to right). Interference voltages  $V_p$  are indicated. Upper inset: frequency dependence of the lowest two interference voltages. Lower inset: schematic geometry of the sample and a single channel. Strong pinning CE's are marked gray. The (local) vortex lattice parameters and (effective) channel width are indicated.

Figure 1 shows a series of IV curves measured at 60 mT with superimposed 6 MHz rf-currents of various amplitudes. The dc-IV curve ( $I_{rf} = 0$ ) shows a nonlinear voltage upturn from which  $I_c$  was determined using a 100 nV criterion. The application of sufficiently large rf-currents leads to clear mode-locking steps at equidistant voltage levels  $V_p$  which are indicated for  $p = 1, 2, 3$ . As shown below,  $q = 1$  and thus  $p = 1$  refers to the fundamental and  $p = 2, 3$  to higher harmonics. These voltage levels depend linearly on  $f$ , as follows for  $p = 1, 2$  from the upper inset to Fig. 1. The interference step width  $\Delta I$  for each harmonic shows Bessel function-like oscillations with  $I_{rf}$  which will be discussed in detail elsewhere.

Next we turn to the field dependence of the mode-locking phenomenon. The characteristics are better displayed by plotting the differential conductance  $dI/dV$  versus  $V$ , as done in Fig. 2 for the  $f = 6$  MHz data. The results shown are obtained at constant  $I_{rf} \simeq 10I_c$  in

fields from 300 mT (bottom) to 60 mT (top) with steps of 10 mT. The interference steps, now appearing as peaks in  $dI/dV$ , change in amplitude and in voltage position with field. Focusing on the fundamental peak at  $V_1$ , it is seen that in certain field intervals  $V_1$  is field independent, e.g. from 60 – 100 mT  $V_1$  is 4.6  $\mu\text{V}$ . At 90 mT another fundamental peak appears at a voltage of 6.9  $\mu\text{V}$ , which lies between the  $p = 1$  and  $p = 2$  interference peaks in lower fields. The second harmonic now coincides with the  $p = 3$  peak at 60 mT. Between 100 and 110 mT, the lower voltage  $p = 1$  peak vanishes while the 6.9  $\mu\text{V}$  peak (and its higher harmonics) grow and remain detectable up to  $\approx 180$  mT.

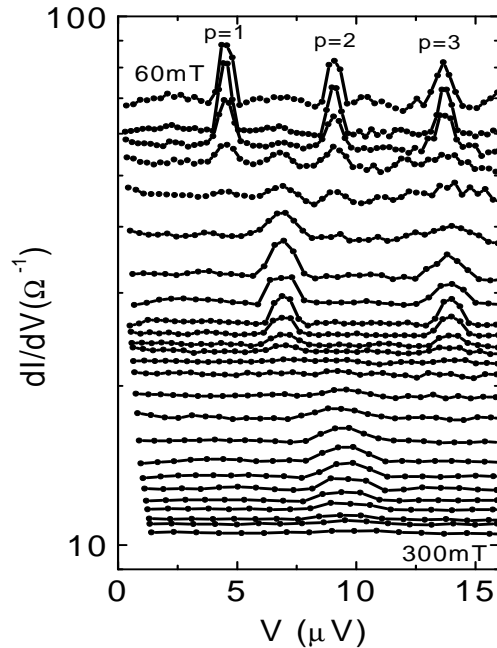


FIG. 2. Differential conductance  $dI/dV$  versus  $V$  as obtained from the IV curves (as in Fig. 1): the applied field is varied from 300 mT (bottom) to 60 mT (top) in steps of 10 mT. The amplitude of the superimposed 6 MHz rf-current is  $I_{rf}/I_c \sim 10$ .

The described sequence of appearances and disappearances of the peaks continues for larger fields. The resulting variation of  $V_1$  with field is shown in more detail in Fig. 3(a). We plot the ratio of  $V_1$  over  $f$  to also include data taken at  $f = 60$  MHz. Both data sets collapse on distinct voltage plateaus separated by abrupt steps. Around the steps two consecutive fundamental interferences can coexist. This behavior is independent of frequency and  $I_{rf}$ . The voltage separation between adjacent plateaus corresponds to the value of  $V_1/f$  of the lowest plateau. Therefore we labelled the plateaus by integers  $n$ . This staircase-like behavior suggests that  $V_1/f$  reflects a process in which the number of vortex rows in each channel changes with field in a discrete manner.

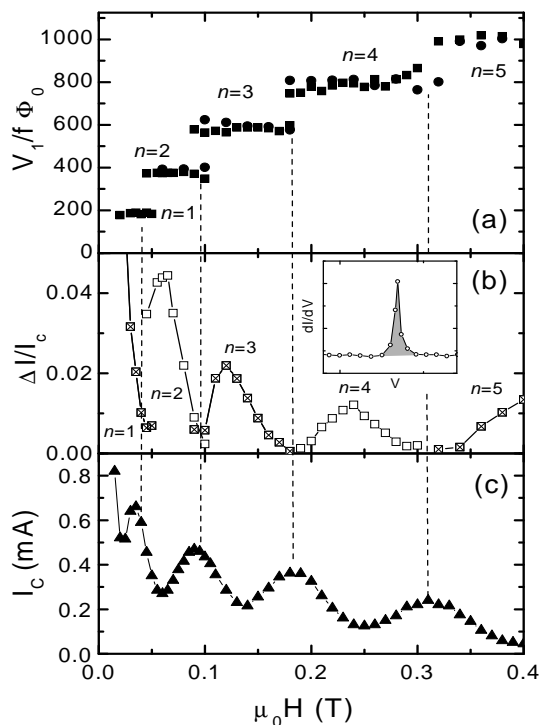


FIG. 3. (a)  $V_1/f$  in units  $\Phi_0$  versus magnetic field  $\mu_0 H$  for 6 MHz ( $\bullet$ ) and 60 MHz ( $\blacksquare$ ). (b) The normalized width of the interference current steps  $\Delta I/I_c$  of the  $V_1$  peaks at 6 MHz. Data belonging to odd  $n$  are cross-marked for clarity.  $\Delta I$  is defined by the gray area in the inset. (c) The field dependence of the depinning current  $I_c$  determined from a 100 nV criterion.

The relation between interference voltage and number of moving rows can be derived as follows: the general interference condition for the velocity of an *ordered* array with *average longitudinal vortex spacing*  $a$  and row spacing  $b$  (see inset to Fig. 1) is  $v_{p,q} = (p/q)fa$ . Thus the interference voltage per channel  $\tilde{V}_{p,q} = w_{eff} B v_{p,q}$ , with  $B = \Phi_0/ab$  the induction, is:

$$\tilde{V}_{p,q} = \frac{p}{q} \Phi_0 f w_{eff} / b = \frac{p}{q} \Phi_0 f n, \quad (1)$$

where  $w_{eff}/b = n$  is the number of moving rows. Taking into account that we measure the voltage  $V$  over  $\sim 200$  channels, the height of the jumps in  $V_1/f$  in Fig. 3(a) corresponds to  $\Phi_0$ , validating the identification of the peaks at  $V_1$  as fundamental. We note that, regardless of field, no subharmonic peaks ( $q \neq 1$ ) could be resolved. Such subharmonics *have* been observed in dc-rf driven charge density waves and bulk vortex lattices [5,14]. Here, their absence might be explained by the fact that our pinning potential, which stems from the interaction with pinned vortices in the CE's with average spacing  $\sim a_0$ , predominantly contains modes with wave vector  $\lesssim 2\pi/a_0$  [12].

The data in Fig. 3(a) combined with Eq. (1) shows unambiguously that in those parts of the flow where vortices show mode locking, the number of moving rows  $n$

changes with field by one. We consider now in more detail the field dependence of the amplitude  $\Delta I$  of the mode locked steps, i.e. the area under the interference peaks (see the inset to Fig. 3(b)). Figure 3(b) shows  $\Delta I$  associated with the voltage plateaus for consecutive  $n$  in (a), normalized by  $I_c$ . At fields around the middle of the plateaus,  $\Delta I/I_c$  is large. This indicates a large degree of coherency in the motion and implies that a unique, integer number of rows  $n$  is moving, corresponding to a matching configuration as in the lower inset to Fig. 1. Approaching the edges of the plateaus,  $\Delta I/I_c$  decreases, signalling a reduction of the coherency in the moving arrays. At the plateau edges,  $\Delta I/I_c$  is strongly suppressed, even if  $I_{rf}$  is varied. The coexistence of a residual signal from  $n$  and  $n \pm 1$  row configurations at the transition fields evidences that these fields correspond to the maximum mismatch situation.

It is clear that upon approaching a mismatch condition, a moving  $n$  row configuration experiences increasing lattice strains which will progressively induce misfit dislocations in the structure. Let us now compare the observed transitions to the oscillations in  $I_c$  in Fig. 3(c). It is seen that *maxima in  $I_c$  appear at the  $n \rightarrow n \pm 1$  transition fields*, while the minima in  $I_c$  are located near matching fields [15]. Therefore we conclude that, upon increasing the density of misfit dislocations in the channel,  $I_c$  is enhanced. This result contrasts the picture in which dislocations lower the flow stress and is strongly reminiscent of the mechanism expected for the traditional peak effect in a random potential.

As mentioned, the positional disorder of vortex arrays in the CE's, which is quenched for fixed field, plays a crucial role for understanding the relation between mismatch and the dc-depinning current  $I_c$ . We address this issue now in more detail by molecular dynamics simulations [11,12] of dc-driven channel vortices in the geometry of the lower inset to Fig. 1. Vortex interactions were modelled by the London potential with  $\lambda/a_0 = 2$  ( $\lambda$  is the penetration depth) [16]. The CE vortices were assigned random shifts  $\mathbf{d}$  with respect to the ideal lattice configuration, such that  $\sqrt{\langle (\nabla \cdot \mathbf{d})^2 \rangle} \simeq 0.12$ . We keep the average orientation of the CE arrays with a principal axis parallel to the channel. The vortex density in the channel and the CE's were both  $(a_0 b_0)^{-1}$ , while the matching condition was tuned by the ratio  $w_{eff}/b_0$ .

First we discuss the results of simulations around matching of a 3 row configuration ( $w_{eff}/b_0 = 3.05$ ). The (rescaled)  $J_c$  obtained in such simulations attains a value  $J_c = 2Ac_{66}/(Bw_{eff}) \equiv (A/A^0)J_c^0$  with  $A \simeq 0.2A^0$  [17] where  $A^0 = (\pi\sqrt{3})^{-1}$  is the theoretical value for shear flow of perfectly matching vortex arrays along ordered CE's [11]. To understand the origin of this reduced flow stress we turn to Fig. 4(a) and (b). In (a) we show vortex trajectories during motion over  $5a_0$  for a dc-drive  $J \simeq 3J_c^0$ . The trajectories are essentially parallel to the CE's and clearly show motion of 3 rows. A Delauney

triangulation (Fig. 4(b)) of a snapshot of (a), shows that vortices in the channel are mostly sixfold coordinated and elastically coupled. However, at the CE's, dislocations are present with Burgers vectors (denoted by arrows) along the flow direction. These dislocations, which are mainly induced by disorder in the CE's, are responsible for the reduction of  $J_c$  with respect to  $J_c^0$ .

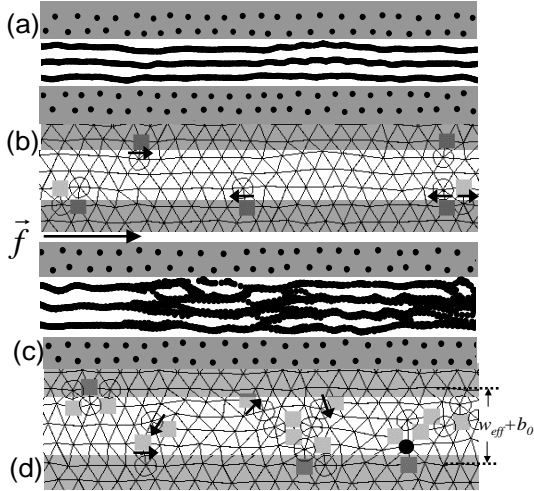


FIG. 4. (a) Flow trajectories during motion over  $5a_0$  around matching ( $w_{eff}/b_0 = 3.05$ ) for  $J \approx 3J_c^0$ . Note the positional disorder in the CE arrays. (b) Delauney triangulation of one snapshot of (a). Direction of the drive  $\vec{f} = \vec{J} \times \vec{\Phi}_0$  is shown and Burgers vectors of the dislocations are indicated by arrows. (c) Trajectories at mismatch ( $w_{eff}/b_0 = 3.55$ ) for  $J \approx 3.5J_c^0$ . (d) Triangulation of a snapshot of (c). All data were taken for a channel of length  $L = 150a_0$  and cyclic boundary conditions.

To study a mismatch situation we consider the case  $w_{eff}/b_0 = 3.55$ . The critical current we find is characterized by  $A = 0.065 \simeq 0.4A^0$ , indeed enhanced compared to matching. Figure 4(c) shows the corresponding trajectories for  $J \approx 3.5J_c^0$ . Here, one observes coexistence of 3 and 4 moving rows and in addition substantial transverse displacements and switching of vortices between rows. Importantly, the 3 and 4 row regions remain quasi-static during motion and their location is determined by static disorder in the CE's. The triangulation in (d) of a snapshot of the flow reveals numerous dislocations *inside the channel*. In contrast to the matching case, their Burgers vectors assume all possible orientations and are mostly misoriented to the flow direction. The motion of these misoriented dislocations is blocked by the interaction with disorder in the CE's and with neighboring misoriented dislocations. This results in quasi-static fault zones where during the flow the dislocation pattern changes irregularly and the vortex trajectories are jammed. These phenomena form the mechanism underlying the enhanced flow impedance at mismatch.

The overall picture that has emerged from these sim-

ulations is that on approaching a matching state, the fault zones gradually heal, yielding a gradual decrease of the critical current. Simultaneously the size of coherent  $n$ -row regions grows, providing an explanation for the experimentally observed increase in the rf-dc interference signal. On changing the field, vortex dynamics in the channels thus exhibits a series of smooth structural transitions from quasi-1D coherent motion to quasi-2D disordered flow in a disordered potential.

In summary, we investigated the flow of vortices in mesoscopic channels bounded by pinned vortices. The rf-dc interference measurements yield unambiguous information on the field evolution of the number of moving rows and coherency in the channel. The depinning current oscillations exhibit maxima at mismatch conditions. Simulations show that this behavior originates from blocking of misoriented dislocations in quasi-static fault zones, which gradually heal on approaching a matching state.

This work was supported by the 'Stichting voor Fundamenteel Onderzoek der Materie' (FOM). N.K. was supported by JSPS. V.M.V. was supported by the DOE Office of Science.

- 
- [1] P.H. Kes and C.C. Tsuei, Phys. Rev. B **28**, 5126 (1983); S. Bhattacharya and M.J. Higgins, Phys. Rev. Lett. **70**, 2617 (1993).
  - [2] O. Daldini *et al.*, Phys. Rev. Lett. **32**, 218 (1974).
  - [3] P. Martinoli, Phys. Rev. B. **17**, 1175 (1978); P. Martinoli *et al.*, Solid State Comm. **17**, 205 (1975).
  - [4] K. Harada *et al.*, Science **274**, 1167 (1996).
  - [5] A. T. Fiory, Phys. Rev. Lett. **27**, 501 (1971); A. Schmid and W. Hauger, J. Low. Temp. Phys. **11**, 667 (1973).
  - [6] L. Van Look, *et al.*, Phys. Rev. B **60**, 6998 (1999).
  - [7] A. M. Troyanovski *et al.*, Nature **399**, 665 (1999).
  - [8] J. M. Harris *et al.*, Phys. Rev. Lett. **74**, 3684 (1995); A. Kolton *et al.*, *ibid.* **86**, 4112 (2001).
  - [9] A. Pruyboom *et al.*, Phys. Rev. Lett. **60**, 1430 (1988); M.H. Theunissen *et al.*, *ibid.* **77**, 159 (1996).
  - [10] The ratio  $I_c^{NbN}/I_c^{NbGe} > 5 \times 10^3$  while  $I_c^{NbN} \simeq 60$ mA.
  - [11] R. Besseling *et al.*, Phys. Rev. Lett. **82**, 3144 (1999).
  - [12] R. Besseling, Ph. D. Thesis, Leiden University (2001); R. Besseling *et al.*, cond-mat/0202485; <http://lions1.leidenuniv.nl/wwwhome/rbessel>.
  - [13] G.J.C. van Baarle *et al.*, to be published.
  - [14] G. Grüner, Rev. Mod. Phys. **60**, 1129 (1988); R. E. Thorne *et al.*, Phys. Rev. B. **35**, 6360 (1987).
  - [15] A device with  $w = 290$ nm showed the same behavior.
  - [16] This interaction yields the correct  $c_{66}$ . The results did not change for a larger ratio  $\lambda/a_0$ .
  - [17] The values  $0.2A^0$  at matching and  $0.4A^0$  at mismatch are in reasonable agreement with the experimental critical current obtained from linear extrapolation of the  $IV$ -curves to  $V = 0$  [12].